

Synth-to-Real Unsupervised Domain Adaptation for Instance Segmentation

Yachan Guo¹, Yi Xiao¹, Danna Xue^{1,2}, Jose Luis Gomez Zurita¹, and Antonio M. López¹

¹ Computer Vision Center, Universitat Autònoma de Barcelona, Spain

² Northwestern Polytechnical University, China

{yguo,yxiao,dxue,jlgomez,antonio}@cvc.uab.es

Abstract. Unsupervised Domain Adaptation (UDA) aims to transfer knowledge learned from a labeled source domain to an unlabeled target domain. While UDA methods for synthetic to real-world domains (synth-to-real) show remarkable performance in tasks such as semantic segmentation and object detection, very few were proposed for the instance segmentation task. In this paper, we introduce UDA4Inst, a model of synth-to-real UDA for instance segmentation in autonomous driving. We propose a novel cross-domain bidirectional data mixing method at the instance level to fully leverage the data from both source and target domains. Rare-class balancing and category module training are also employed to further improve the performance. It is worth noting that we are the first to demonstrate results on two new synth-to-real instance segmentation benchmarks, with 39.0 mAP on UrbanSyn \rightarrow Cityscapes and 35.7 mAP on Synscapes \rightarrow Cityscapes. UDA4Inst also achieves the state-of-the-art result on SYNTHIA \rightarrow Cityscapes with 31.3 mAP, +15.6 higher than the latest approach. Our code will be released.

Keywords: Unsupervised Domain Adaptation · Instance Segmentation · Synth-to-Real

1 Introduction

Instance segmentation provides a detailed and fine-grained understanding of the objects in an image, which is critical for a variety of real-world applications, such as multi-object tracking [2, 29, 48], pose estimation [1, 5], motion prediction [35, 63]. Specifically, in autonomous driving, the segmentation of instance objects is useful as it helps to locate safety-critical objects (such as pedestrians or riders) with accurate boundaries, enabling more advanced scene analysis and decision-making in many scenarios [2, 8, 58, 65].

However, in practice, training instance segmentation models requires access to a large amount of densely labeled data. Each instance needs to be accurately delineated with pixel-level masks, which is laborious and highly time-consuming. In addition, in order to ensure a proper model generalization, the data must contain a wide range of object appearances, poses, scales, and backgrounds.

Therefore, the label acquisition and object variability needed for instance segmentation encounter a data-hungry bottleneck in the real-world domain. This challenge demands a more intelligent approach to enhance the efficiency of the labeling of instance segmentation data.

As an alternative, synthetic data is increasingly being used for deep learning applications as it enables large-scale training data for models of vision tasks [45]. Synthetic data offers labels annotated in a more time- and resource-efficient way, as it is directly generated by simulators [11, 44] along with images. Crucially, it allows for the incorporation of diversity into the training dataset, thereby enhancing the model’s generalization capability. Moreover, synthetic data can be tailored to produce scenarios that are rare in the real world.

Utilizing synthetic data to replace real-world data for model training is based on the premise that training and test samples are drawn from the same distribution. Unfortunately, the distribution of these two domains of data is different (*i.e.* a domain gap does exist). UDA methods are essential for mitigating the inherent domain gap between the synthetic source and the real-world target domains. In recent years, many studies have explored the integration of synthetic data and UDA methods to address a wide range of computer vision tasks including image classification [12, 39, 40, 42, 47], object detection [14, 16, 43, 46, 54, 67], and semantic segmentation [3, 17, 20, 24, 25, 28, 38]. Comparatively, there has been relatively little research on UDA for instance segmentation, which is reflected in only three works [27, 52, 70] in the last five years. Among them, although [27, 52] do provide results on instance segmentation, they were models designed for the panoptic segmentation task, and [70] was based on a suboptimal MaskR-CNN framework with adversarial learning.

In this paper, we focus on designing a novel synth-to-real **UDA** model for **Instance Segmentation (UDA4Inst)** following an online self-training pattern. We employ the advanced universal segmentation model Mask2Former [6] to demonstrate the effectiveness of our proposed UDA method. Unlike the previous models [13, 26, 30, 56] that only perform a unidirectional cross-domain data mixing, *i.e.* either source-to-target (S2T) or target-to-source (T2S), UDA4Inst employs a new bidirectional cross-domain data mixing based on instance objects. We show that our strategy improves the mAP results over the unidirectional ones. Furthermore, to address the ubiquity of the class imbalance problem in the existing datasets, UDA4Inst is equipped with a novel algorithm that can online balance rare-class instances during cross-domain data mixing. In this way, we observe a clear improvement in the segmentation for rare-class instance objects, which contributes to a better generalization of the model. As the third methodological contribution, we explore category module training where multiple classes are categorized into several modules for separate training, and the final results consist of the output from each module. Last but not least, we demonstrate the effectiveness of UDA4Inst on three UDA instance segmentation benchmarks. To the best of our knowledge, we are the first to perform UDA instance segmentation with synthetic datasets of UrbanSyn [15] and Synscapes [66], reaching respectively 39.0 mAP and 35.7 mAP on Cityscapes. Our results on SYNTHIA-

to-Cityscapes reach the state-of-the-art with 31.3 mAP (56.9 mAP50), +15.6 (+22.6) higher than the previous best record [52].

2 Related Work

2.1 Instance Segmentation

Early mainstream deep learning models based on convolutional neural networks (CNNs) for instance segmentation, such as MaskR-CNN [21] and YOLACT [4] have achieved remarkable successes. In recent years, with the adoption of the self-attention mechanism in natural language processing [60] and computer vision [10, 49, 71], transformer-based models [6, 7, 31, 34] have emerged and surpassed CNN-based architectures in many tasks such as object detection [34], semantic segmentation [6, 7, 31, 34], and panoptic segmentation [6, 7, 31, 34]. Among them, Mask2Former [6] has attracted great attention as a universal architecture that obtains top results in three major image segmentation tasks (panoptic, instance, and semantic) on benchmarks. It introduces masked attention, which extracts localized features by constraining cross-attention within predicted mask regions. In this work, we leverage this advanced universal segmentation architecture to prompt the state-of-the-art results in instance segmentation with UDA.

2.2 Unsupervised Domain Adaptation

Typically, UDA designed for major computer vision problems occupy three groups: domain discrepancy alignment, adversarial learning, and self-training. In domain discrepancy alignment, a proper divergence measure, such as maximum mean discrepancy [51], correlation alignment [55], or Wasserstein distance [37] is chosen as a measure to minimize domain discrepancy in a latent feature space. Adversarial learning approaches [18, 22, 23, 53, 57, 61] aims to achieve domain invariance in rather input space, feature extraction, or output space. Instead of reducing domain discrepancy with a divergence measure, self-training methods [24–26, 56, 64] iteratively learn a segmentation model by generating and assigning pseudo-labels to model training in the unlabeled target domain. DaFormer [24] proposes a transformer-based domain adaptation model, effectively handling multi-domain data by introducing domain attention and adversarial training mechanisms. HRDA [25] is a model designed for domain adaptation in high-resolution images, enhancing domain adaptation performance through the integration of hierarchical attention and multi-resolution representations. MIC [26] leverages masked image consistency to enhance context understanding for generalization. In this work, our proposed solution follows the pattern of **self-training**, assigning pseudo-labels to unlabeled training examples through a model learned by the labeled data, and iteratively including them in the learning process.

Specifically, the main purpose of this work is to explore UDA for instance segmentation in the field of autonomous driving. Previous work exploring UDA

methods for image segmentation tasks mainly focuses on semantic segmentation [24, 25, 28]. Recently, some work on UDA for panoptic segmentation [27, 52] has been proposed that can simultaneously achieve domain-adaptive instance and semantic segmentation within a single network. Nevertheless, they are not designed for instance segmentation. The most related to our work is [70], which also aims to address the challenge of synth-to-real domain adaptation for instance segmentation. It consists of three feature adaptation modules at different levels (global, local, and subtle), and the training process was based on discriminator networks with adversarial learning. However, this work adopts the MaskR-CNN framework, whose performance might be limited by the CNN architecture and the R-CNN framework designed for the object detection task, thus leading to non-ideal results compared to transformer-based models. In contrast, we focus on designing a synth-to-real UDA framework following the self-training pattern with an advanced transformer-based segmentation network Mask2Former.

2.3 Cross-domain Data Mixing

A commonly used data augmentation technique for classification and semantic segmentation tasks is mixing [33]. There are two main types of mixing: soft mixing [13, 19, 69] and hard mixing [25, 30, 32, 56, 59, 62, 68]. The former one obtains mixed images by pixel-wise weighted average of two images, while the latter extracts patches from other image and pastes it to the current image. In UDA, this augmentation is usually applied in the form of cross-domain data mixing, *i.e.* the mixed samples consist of data from both source and target domains. Tranheden *et al.* introduce DACS [56], a unidirectional cross-domain data mixing strategy that cuts out semantic pixels in the source domain and pastes them into samples in the target domain. This strategy is further applied in subsequent research [25]. Gao *et al.* propose a dual soft-paste strategy that not only considers mixing data from the source to target images but also within the source domain itself [13]. A similar idea is suggested by Huo *et al.*, while for the dual mixing [30], they focus on the target-to-target domain. Our proposed strategy differs from the aforementioned papers in applying a bidirectional domain mixing which includes both S2T and T2S directions. Our intuition is that incorporating T2S data mixing can bootstrap the model to better learn features in the target domain, thereby improving domain adaptation performance. Most recently, Kim *et al.* also propose a bidirectional cut-and-paste strategy based on image patches [32]. The main difference between our strategy and theirs is that we cut out instance objects instead of image patches. We believe that instance-based data mixing can reduce the impact of redundant background features on instance segmentation compared to patch-based ones.

3 Methodology

3.1 Overall Approach

For the source domain dataset \mathcal{D}_S , comprising images X_S and their instance labels Y_S , an instance segmentation model f_θ can be trained in a supervised

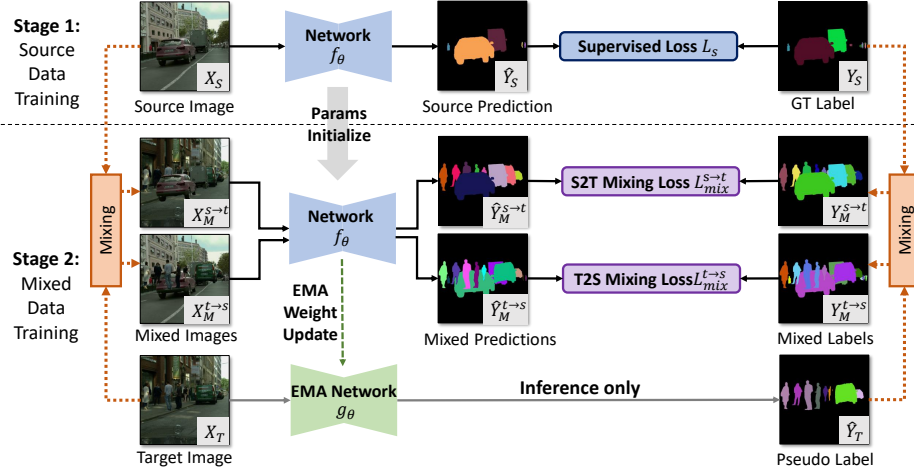


Fig. 1: Overview of our proposed UDA4Inst framework. In the first stage, the student network is trained with source domain data in a supervised manner. In each iteration of the second stage, we update the EMA teacher g_θ with the weights from the network f_θ to predict pseudo-labels in the target domain. Next, the mixed data are generated with the source and target images, and the mixed labels are generated by the target pseudo-labels and the source ground-truth labels. The network is then trained on the mixed data with S2T and T2S mixing losses.

manner. However, the target domain dataset \mathcal{D}_T only provides unlabeled images X_T . We aim to address the domain gap by leveraging X_S , Y_S , and X_T to train a model capable of accurately predicting object instances on X_T .

As shown in Fig. 1, our UDA framework is based on online self-training. The training has two stages. In the first stage, the model f with parameters θ is trained on the source domain in a supervised manner for T_{stage1} iterations, with synthetic images X_S and their corresponding ground-truth labels Y_S . Our goal is to minimize a supervised segmentation loss

$$\mathcal{L}_{stage1} = \mathcal{L}_{seg}(\hat{Y}_S, Y_S), \quad (1)$$

then the network can be used to predict pseudo-labels on target domain \hat{Y}_T . In our case, we use an advanced universal image segmentation architecture, Mask2Former [6], as the base network for instance segmentation. The segmentation loss for Mask2Former is

$$\mathcal{L}_{seg} = \lambda_{ce} \mathcal{L}_{ce}(\hat{Y}, Y) + \lambda_{bce} \mathcal{L}_{bce}(\hat{Y}, Y) + \lambda_{dice} \mathcal{L}_{dice}(\hat{Y}, Y), \quad (2)$$

where binary cross-entropy loss \mathcal{L}_{bce} and dice loss \mathcal{L}_{dice} is for binary mask segmentation, \mathcal{L}_{ce} is for instance class classification. λ_{bce} , λ_{dice} and λ_{ce} are the hyper-parameters.

In the second stage, we utilize the cross-domain bidirectional mixed images and labels produced by both source and target domain data to resume the training of the model f_θ for T_{stage2} iterations. The rare-class instances in the source

Algorithm 1 Our UDA4Inst algorithm

Require: Source domain datasets $\{X_S^i, Y_S^i\}_{i=1}^{N_S}$, target domain dataset $\{X_T^j\}_{j=1}^{N_T}$, iterations for stage1 and satge2 T_{stage1}, T_{stage2} , instance segmentation model f_θ , and EMA teacher model g_θ

- 1: **for** $iter = 1$ to $iter = T_{stage1}$ **do**. ▷ Stage 1: source data training
- 2: Compute prediction, $\hat{Y}_S \leftarrow f_\theta(Y_S)$.
- 3: Compute supervised loss, $\mathcal{L}_{stage1}(\hat{Y}_S, Y_S)$.
- 4: Compute gradients, $loss.backward()$.
- 5: Update f_θ weights, $optimizer.step()$.
- 6: **end for**
- 7: **for** $iter = 1$ to $iter = T_{stage2}$ **do** ▷ Stage 2: mix data training
- 8: Update the parameters of EMA teacher $g_\theta \leftarrow f_\theta$.
- 9: Generate pseudo-labels for target images $\hat{Y}_T \leftarrow g_\theta(X_T)$.
- 10: Generate mixing images and labels $X_M^{s \rightarrow t}, Y_M^{s \rightarrow t}, X_M^{t \rightarrow s}, Y_M^{t \rightarrow s} \leftarrow$ Augmentation, bidirectional mixing X_S, Y_S, X_T, \hat{Y}_T , and rare class sampling
- 11: Compute prediction, $\hat{Y}_M^{s \rightarrow t} \leftarrow f_\theta(X_M^{s \rightarrow t}), \hat{Y}_M^{t \rightarrow s} \leftarrow f_\theta(X_M^{t \rightarrow s})$.
- 12: Compute mix losses, $\mathcal{L}_{stage2}(\hat{Y}_M^{s \rightarrow t}, \hat{Y}_M^{t \rightarrow s}, Y_M^{s \rightarrow t}, Y_M^{t \rightarrow s})$.
- 13: Compute gradients, $loss.backward()$.
- 14: Update f_θ weights, $optimizer.step()$.
- 15: **end for**
- 16: **return** f_θ

domain are resampled during data mixing. Since the target images X_T are unlabeled, we utilize the pseudo-labels generated by the exponential moving average (EMA) teacher model g_θ . At the beginning of the second stage, the parameters of the EMA teacher are initialized by the weights of f_θ . Then, in each training step, we first infer the target images by the EMA teacher to get pseudo-labels \hat{Y}_T . In line with common practice [9, 24–26, 56], we use confidence thresholds to filter out noisy pseudo-labels. A pseudo-label confidence score is calculated as the product of *mask confidence* (confidence of whether an instance object exists in a mask) and *class confidence* (confidence of an instance class). Then, we leverage the ground-truth labels Y_S and the pseudo-labels \hat{Y}_T to perform bidirectional instance cut-and-paste, thereby obtaining mixed data $X_M^{s \rightarrow t}, Y_M^{s \rightarrow t}, X_M^{t \rightarrow s}, Y_M^{t \rightarrow s}$. Finally, mixed data are used to train the model f_θ with a weighted bidirectional data mixing loss

$$\mathcal{L}_{stage2} = \lambda_{mix}^{s \rightarrow t} \mathcal{L}_{seg}(\hat{Y}_M^{s \rightarrow t}, Y_M^{s \rightarrow t}) + \lambda_{mix}^{t \rightarrow s} \mathcal{L}_{seg}(\hat{Y}_M^{t \rightarrow s}, Y_M^{t \rightarrow s}), \quad (3)$$

where $\lambda_{mix}^{s \rightarrow t}$ and $\lambda_{mix}^{t \rightarrow s}$ are weights for different directional mixing data. Then the EMA teacher parameters are updated. Algorithm 1 illustrates the flow of our proposed approach in detail.

Bidirectional Data Mixing. In data mixing, the mixed images are generated by cut-and-paste image regions from one image to another. Different from DACS [56] which only performs unidirectional data mixing in the S2T direction (see Fig. 2a), we propose an instance-level bidirectional data mixing strategy

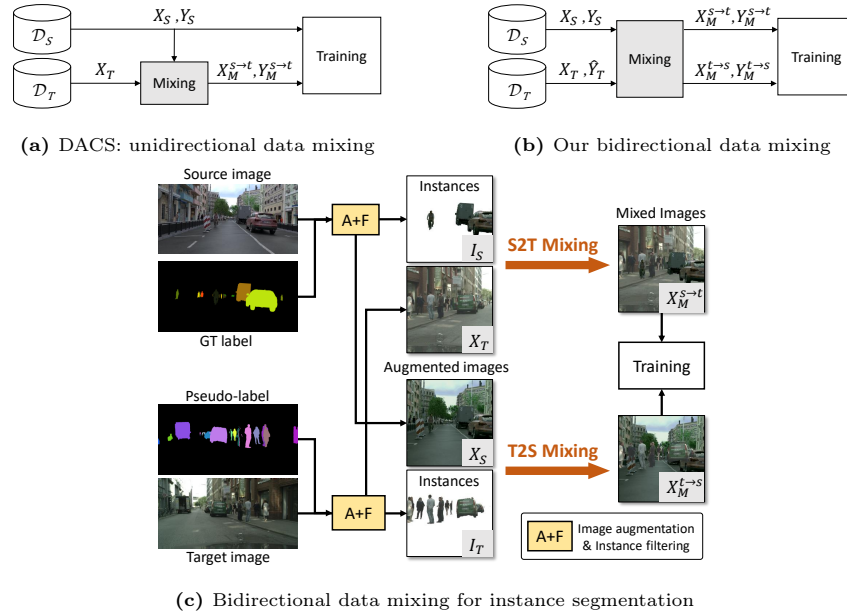


Fig. 2: Comparison between Uni- and Bi-directional data mixing strategies. Compared to DACS which only applies S2T data mixing, our UDA4Inst conducts bidirectional data mixing in both S2T and T2S manner to make the model learn better features from target instances. In bidirectional data mixing, the mixed images and labels are generated by cutting the instances from either the source or target domain, and pasting them to images in another domain.

that fully utilizes instances from both source and target domains (see Fig. 2b). As shown in Fig. 2c, in each iteration of the mixed data training stage, the mixed data is generated in both S2T and T2S directions. For S2T mixing, the instances in a source domain image X_S are cut and pasted onto a target domain image X_T , resulting in an augmented mixing images $X_M^{s \rightarrow t}$. Its corresponding instance label $Y_M^{s \rightarrow t}$ is created according to the image, where the instance labels are added to the generated target pseudo-labels \hat{Y}_T . Similarly, to obtain the T2S mixing data $X_M^{t \rightarrow s}$ and $Y_M^{t \rightarrow s}$, we leverage the generated pseudo-labels of the target images \hat{Y}_T to mask out the instances that are desired to be pasted on the source image X_S . The network is trained on mixed images $X_M^{s \rightarrow t}, X_M^{t \rightarrow s}$ with mixed labels $Y_M^{s \rightarrow t}, Y_M^{t \rightarrow s}$. Compared to using image patches for mixing, we use instance-based data mixing to avoid the impact of redundant background, leading to a more realistic mixed image. We provide rich experimental results in Sec. 4 to demonstrate the effectiveness of our proposed bidirectional data mixing strategy.

Category Module Training. Conventionally, the instance class labels have specific semantic meanings such as: ‘Motorcycle’, ‘Bicycle’, ‘Train’ *etc.* Instances with similar semantics tend to have more common features. For example, ‘Mo-

torcycle - Bicycle’ may contain more common features than ‘Train - Bicycle’, therefore leading to a higher inter-class correlation. Based on this inductive bias, we propose category module training. Instead of training one model to predict all classes, we separate the classes into several category groups. We train one model for each group and combine the outputs of these models to obtain the final result. Our assumption is that introducing this inductive bias may guide the model to better learn and associate the inter-class and intra-class features. We provide rich ablation study results in Sec. 4 to verify the idea. Note that in this work, we consider the number of category groups to two, to verify the profit of the proposed category module training.

Rare-class Balancing. Class imbalance has a negative impact on the performance of deep learning models. Since the goal of model training is to minimize the overall error, models trained on datasets with obvious class imbalance tend to be biased toward the classes with large amounts of data, resulting in poor performance on the classes with few data. In our three synthetic datasets, we observe that there exists a class imbalance problem. Therefore, we want to increase the training frequency of instances from these rare classes by intentionally cutting and pasting them in data mixing. In each category group, for the class that occupies the smallest percentage of instances, we define it as a rare class: ‘Motorcycle’ and ‘Train’ for UrbanSyn (2.47% and 0.37%) and Synscapes (5.91% and 2.55%), ‘Motorcycle’ and ‘Bus’ for SYNTHIA (2.18% and 2.08%).

Fig. 3 demonstrates the operation of our proposed rare-class balancing. Specifically, during the process of traversing images for data mixing, for those images containing rare-class instances, we store these images and the corresponding instance labels in a pool with a maximum number of sample N . These N samples in the pool are continuously updated with newly emerged rare-class instance objects and their corresponding images in a FIFO (first-in, first-out) fashion. In turn, when encountering images that do not contain rare classes, we randomly select half of the samples in the pool and mix them on these images. To avoid error accumulation from pseudo-labels, we only apply rare-class balancing to data mixing in the S2T manner. Note that the whole process is done online, thus no pre-processing is required.

4 Experiments

4.1 Datasets

In the experiments, we set Cityscapes [8] as the target domain, and UrbanSyn [15], Synscapes [66] and SYNTHIA [50] as source domains. We conduct experiments in three synth-to-real domain settings: UrbanSyn \rightarrow Cityscapes, Synscapes \rightarrow Cityscapes, and SYNTHIA \rightarrow Cityscapes.

Cityscapes is a street-scene dataset that contains 5000 images (2,975, 500, and 1,525 images for training, validation, and testing, respectively) and their corresponding labels for 19 semantic classes and 8 instance classes. Cityscapes is

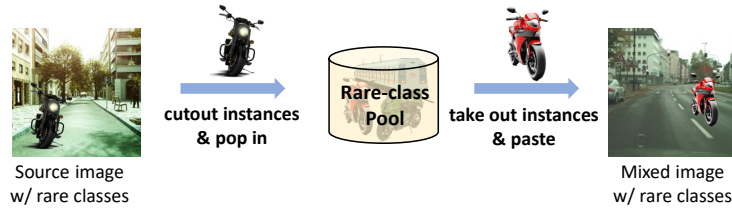


Fig. 3: Our proposed rare-class balancing strategy. During training, in a source image with rare-class instances, we cut out the instances and store them in the rare-class pool. For the target image without any rare classes, we take out instances of the pool and paste them on the target image. This strategy effectively increases the sampling frequency of rare classes without requiring significant memory during training.

a commonly used real-domain dataset with high-resolution (2048×1024) images in the field of autonomous driving.

UrbanSyn is a high-quality synthetic dataset tailored to urban driving scenarios. It comprises a total of 7,539 images with a resolution of 2048×1024 pixels. The images in this dataset have highly realistic rendering effects, making them closely resemble real-world scenes. UrbanSyn has the same instance and semantic classes as Cityscapes.

Synscapes is another physic-based-rendered urban scenes dataset, which includes 25,000 images at a resolution of 1440×720 . The labeled data covers 8 instance classes, but the division is different from Cityscapes. To make them consistent with Cityscapes, we reclassify the ‘Motorcyclist’ and ‘Bicyclist’ instances into ‘Motorcycle’, ‘Bicycle’, and ‘Rider’ leveraging semantic labels. Additionally, we filter the instances with high occlusion, high truncated, or a tiny area during training.

SYNTHIA consists of photo-realistic images in a resolution of 960×720 rendered from a virtual city, with a subset compatible with Cityscapes. This subset contains 9,400 images with pixel-level semantic annotations. SYNTHIA covers 6 classes of instance annotation in Cityscapes, missing ‘Train’ and ‘Truck’.

4.2 Implementation Details

Training We adopt Mask2Former [6] with Swin Transformer [38] backbone pre-trained on COCO [36] as our base network f_θ . To minimize the color discrepancy between the source and target domains, we adopt the same image pre-processing as [20], aligning the style of source domain images to the target one by shifting the distribution of pixel values in CIELAB color space. For image processing, we apply the same data augmentation (flipping, random cropping, *etc.*) as [6] and set the image crop size to 1024×1024 . The maximum number of samples N for the rare-class pool is set to 10, and the pseudo-label confidence threshold τ is 0.9. We set the numbers of iterations for source domain training T_{stage1} to 10k, while the mixed data training T_{stage2} is 20k iterations. For each stage of training, we set a batch size $B=3$ considering optimal memory usage. We use AdamW [41]

Model	AP									AP50								
	Person	Rider	Car	Truck	Bus	Train	M.C	B.C	mAP	Person	Rider	Car	Truck	Bus	Train	M.C	B.C	mAP50
upper bound	41.1	32.4	61.4	44.8	67.5	50.7	26.8	26.6	43.9	75.4	71.3	87.2	58.7	80.3	76.1	58.1	65.1	71.5
UrbanSyn \rightarrow Cityscapes																		
w/o UDA	25.1	19.5	39.8	37.6	51.5	46.7	19.2	16.2	32.0	52.0	48.4	61.5	48.6	66.2	70.0	42.6	46.0	54.4
UDA4Inst	30.0	26.4	49.2	42.9	64.4	58.1	21.3	19.7	39.0	60.1	60.7	75.1	56.4	78.0	77.8	48.7	53.6	63.8
Synscapes \rightarrow Cityscapes																		
w/o UDA	27.2	19.2	39.5	24.0	46.7	33.1	18.7	16.6	28.1	53.9	44.3	67.8	31.9	60.6	58.1	39.9	45.4	50.2
UDA4Inst	30.3	27.1	47.5	34.5	58.5	46.3	22.3	19.1	35.7	59.9	63.2	77.9	45.3	72.8	63.5	46.1	51.7	60.1
SYNTHIA \rightarrow Cityscapes																		
Zhang [70]	9.4	3.8	22.2	-	23.5	-	3.2	2.4	10.8	28.8	17.8	39.9	-	37.5	-	12.8	11.9	24.8
CVRN [27]	-	-	-	-	-	-	-	-	-	34.4	25.3	38.7	-	38.1	-	10.1	8.7	25.9
EDAPS [52]	23.5	13.4	27.5	-	23.6	-	5.8	0.1	15.7	53.9	40.6	50.5	-	38.8	-	21.1	0.7	34.3
w/o UDA	26.3	15.2	38.3	-	43.0	-	13.6	10.9	24.6	53.4	40.8	68.1	-	56.5	-	36.4	36.1	48.6
UDA4Inst	28.1	19.6	47.9	-	58.7	-	18.5	15.0	31.3	57.7	52.5	76.9	-	68.6	-	42.6	43.3	56.9

Table 1: The Instance segmentation performance (AP and AP50) on the three different UDA benchmarks. Zhang [70], CVRN [28] and EDAPS [52] are the related work provide only results in the SYNTHIA \rightarrow Cityscapes setting.

optimizer with an initial learning rate of 0.0001 and a weight decay of 0.05, as well as the learning rate warm-up and the ‘poly’ learning rate schedule. The hyper-parameters of loss λ_{bce} , λ_{dice} , and λ_{ce} are set to 5.0, 5.0, 2.0 respectively. For three synth-to-real settings, we set the weights of bidirectional data mixing loss $\lambda_{mix}^{s \rightarrow t}$, $\lambda_{mix}^{t \rightarrow s}$ to: 0.4, 0.6 for UrbanSyn \rightarrow Cityscapes and SYNTHIA \rightarrow Cityscapes, 0.75, 0.25 for Synscapes \rightarrow Cityscapes. Our model is trained with 3 NVIDIA A40 GPUs, each with 40GB of memory.

Evaluation We evaluate the UDA performance of 8-class instance segmentation on the validation set of Cityscapes. Following the conventional evaluation criteria of instance segmentation, we take AP (Average Precision) and AP50 (Average Precision at IOU=0.5) for each class as our metrics for comparison, and compute the mAP (mean Average Precision) and mAP50 (mean Average Precision at IOU=0.5) for all classes. All the numbers present in the tables are in %.

4.3 Experimental Results

UDA performance. In Table 1, we summarize the results of models tested on the Cityscapes validation set. The table is categorized into two sections showing AP (left) and mAP (right) results, with each section organized from top to bottom into three synth-to-real settings. In all settings, we show results of the UDA4Inst model and the original instance segmentation baseline model Mask2Former [6] trained only on the source dataset. The purpose is to compare the performance difference in domain adaptation when training the same network with or without our proposed UDA method.

To establish an upper bound, we retrain the Mask2Former model on the Cityscapes training set, reproducing similar validation results reported in their paper. It reflects the instance segmentation performance of models trained and

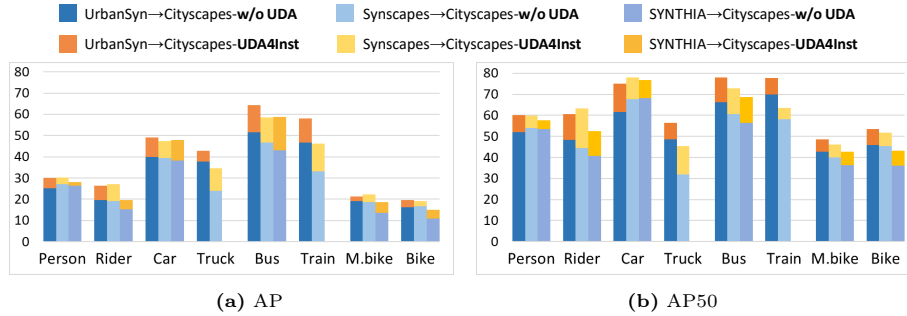


Fig. 4: Comparison of class-wise AP and AP50 between UDA4Inst and the baseline model without UDA. UDA4Inst shows evident improvements in all three synth-to-real settings.

tested on the target domain, *i.e.* without crossing domains. Overall, the first observation is that in all synth-to-real settings, UDA4Inst exhibits a significant improvement in both mAP and mAP50 compared to the baseline model. The most evident improvement is reflected in the setting of Synscapes \rightarrow Cityscapes, where the mAP and mAP50 increased by +7.6 and +9.9 points respectively. Our model achieves the highest 39.0 mAP in UrbanSyn \rightarrow Cityscapes, 35.7 mAP in Synscapes \rightarrow Cityscapes, and 31.3 mAP in SYNTHIA \rightarrow Cityscapes, which are very competitive. Among three settings, we observe that both UDA4Inst and the baseline show better adaptation performance in UrbanSyn \rightarrow Cityscapes. We hypothesize that these results reflect a smaller domain gap between UrbanSyn and Cityscapes.

In particular, UDA4Inst demonstrates consistent enhancement over the baseline model across all the classes in all synth-to-real settings, showcasing the strong efficacy of our proposed UDA method. To intuitively demonstrate the performance difference between these two models, we provide bar charts of class-wise AP and AP50 results in Fig. 4. We can see the gains of UDA4Inst over the baseline one. Notably, in UrbanSyn \rightarrow Cityscapes setting, UDA4Inst achieves 58.1 AP and 77.8 AP50 on the class of ‘Train’, which surpasses the upper bound model with gains of +7.4 and +1.7. It is also worth noting that for the classes of ‘Truck’ and ‘Bus’, UDA4Inst shows very close AP and AP50 results to the upper bound.

As a reference, at the bottom of the table, we also report results from Zhang [70], CVRN [27], and EDAPS [52] that were previously proposed in recent years to address UDA for instance segmentation in SYNTHIA \rightarrow Cityscapes setting. Overall, our proposed UDA4Inst outperforms the other relevant work with a significant improvement, specifically shown as gains of +20.5, +15.6 mAP compared to Zhang and EDAPS, as well as gains of +32.1, +31, +22.6 mAP50 compared to Zhang, CVRN, and EDAPS respectively. Note that we are the first to conduct experiments in the synth-to-real settings of UrbanSyn \rightarrow Cityscapes and Synscapes \rightarrow Cityscapes for instance segmentation.

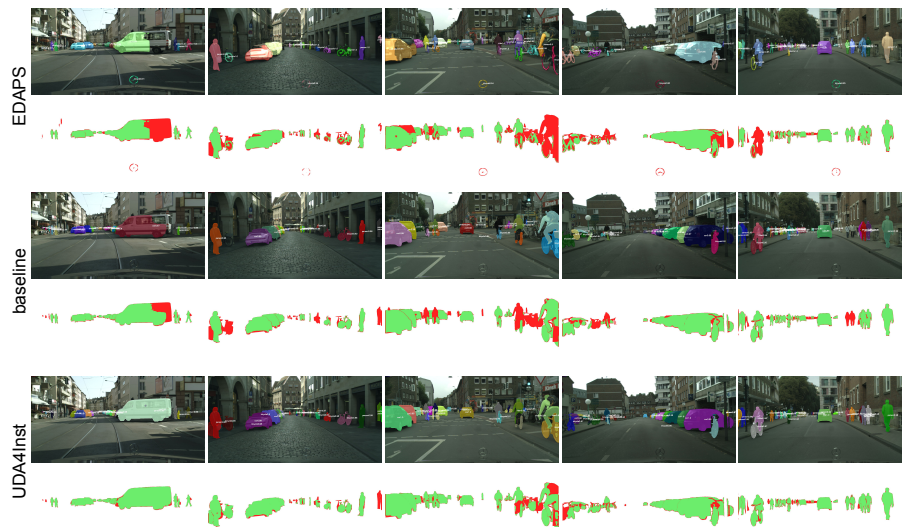


Fig. 5: Qualitative comparison of instance segmentation in the SYNTHIA \rightarrow Cityscapes setting. From top to bottom, we show three sets of quantitative results: 1) the panoptic segmentation model EDAPS, 2) the baseline model without UDA applied, and 3) our UDA4Inst. For each model, we show the instance segmentation predictions overlapped on RGB images and the error maps of semantic results. The **green** areas indicate the correct prediction while the **red** areas indicate the error parts compared to the ground truth.

To further qualitatively demonstrate the performance, in Fig. 5, we visualize the instance segmentation predictions and the error maps of the EDAPS, the baseline model, and UDA4Inst in the SYNTHIA \rightarrow Cityscapes setting. UDA4Inst shows the best segmentation performance, reflected in the fewest error predictions on objects such as cars, riders, and persons. This is consistent with the conclusion drawn from the results in Table 1.

Bidirectional Data Mixing. The results in the UrbanSyn \rightarrow Cityscapes setting are shown in Table 2. The first row presents the results of a baseline model without applying data mixing. The mAP results reveal both S2T and T2S data mixing contribute to a better segmentation performance. T2S is slightly inferior to S2T, which we believe is because the imperfect generated target pseudo-labels can inevitably cause interference in data mixing. Not surprisingly, when combining S2T and T2S, our approach achieves the best result of 37.18 mAP, +5.23 higher than the plain model without data mixing. Only applying S2T mixing neglects the instances in target images. Through bidirectional data mixing, we strike a balance between learning target features and mitigating the negative impact of incorrect target instances on the model. Then, we perform hyperparameters searching for the weights of the BDM loss when applying all three

UDA methods. The results are shown in Table 3. The best result yields at the setting of $\lambda_{mix}^{s \rightarrow t} = 0.4$ and $\lambda_{mix}^{t \rightarrow s} = 0.6$.

Mixing Strategy	mAP	$\lambda_{mix}^{s \rightarrow t}$	$\lambda_{mix}^{t \rightarrow s}$	mAP
w/o mixing	31.95	-	-	34.80
S2T mixing	36.07	0.75	0.25	38.76
T2S mixing	35.00	0.5	0.5	38.09
bidirectional mixing	37.18	0.4	0.6	38.99

Table 2: Ablation study on data mixing strategy. **Table 3:** Hyper-parameters searching for the weights of the BDM loss

To illustrate the advantages of our proposed Bidirectional Data Mixing (BDM) method compared to the unidirectional one, we conduct experiments on different data mixing strategies without applying Rare-class Balancing (RcB) and Category Module Training (CMT).

Category Module Training. As we mentioned, we perform CMT in the hope that introducing this inductive bias can guide the model to better learn the features in classes. To validate our conjecture, in the UrbanSyn \rightarrow Cityscapes setting, we perform CMT on two category groups, which are random compositions of classes (setting 2-5 in Table 4). We also conduct an experiment of full-class training for comparison (setting 1). Overall, we observe that all four CMT models outperform the full-class training one. The best set of category groups is setting 5, which achieves the highest improvement of +3.5 mAP and +5.0 mAP50 compared to the model without applying CMT. We take this group setting as our default setting to conduct the rest experiments.

Component Ablation. To inspect the impact of components of UDA4Inst, we provide an ablation study in the UrbanSyn \rightarrow Cityscapes setting. Specifically, our interest focuses on the three components: BDM, RcB, and CMT. In Table 5, we present mAP results for models that trained without, with some, or with all three UDA methods. The ablative models are named from M1 to M5 (from top to bottom) for illustration.

Overall, we find that the M1 trained without applying any UDA method obtains the lowest mAP of 32.0 among all models. On the contrary, the M6, which is trained with all three UDA methods, achieves the highest score of 39.0. When comparing M1 and M2, we see that applying CMT can effectively improve the model performance by +2.8 mAP gains. The conclusion is further strengthened through the comparison of M3 and M4, where we observe a mAP gain of +1.6 when applying CMT. The effect of BDM is reflected in the performance difference between M1 and M3, where we see that it helps to improve the segmentation results from 32.0 to 36.1 mAP (+4.1 gains). Moreover, under the same circumstance of using CMT, BDM helps to improve the segmentation precision in M4

Setting	Category Groups	mAP	mAP50
1	{Person, Rider, Motorcycle, Bicycle, Car, Truck, Bus, Train}	32.0	54.4
2	{Person, Rider, Bus, Motorcycle}, {Car, Truck, Train, Bicycle}	33.9	57.8
3	{Person, Rider, Car, Bicycle}, {Truck, Bus, Train, Motorcycle}	35.0	59.4
4	{Person, Rider}, {Car, Truck, Bus, Train, Motorcycle, Bicycle}	35.1	59.3
5	{Person, Rider, Motorcycle, Bicycle}, {Car, Truck, Bus, Train}	35.5	59.4

Table 4: Ablation study on category module training. The category groups are defined by classes in brackets.

	CMT	BDM	RcB	Person	Rider	Car	Truck	Bus	Train	M.C	B.C	mAP
M1	-	-	-	25.1	19.5	39.8	37.6	51.5	46.7	19.2	16.2	32.0
M2	✓	-	-	25.2	20.7	47.0	40.2	60.1	52.0	17.1	16.1	34.8
M3	-	✓	-	27.7	23.2	44.2	42.3	61.7	52.7	21.2	15.5	36.1
M4	✓	✓	-	28.9	27.6	50.0	43.6	63.7	47.3	19.5	20.7	37.7
M5	✓	✓	✓	30.0	26.4	49.2	42.9	64.4	58.1	21.3	19.7	39.0

Table 5: Component ablation on proposed UDA method: Category Module Training (CMT), Bidirectional Data Mixing (BDM), and Rare-class Balancing (RcB). ✓ and - indicate whether the component has been applied or not, respectively.

within most of the classes compared to M2, which contributes to a better mAP (+2.9 gains). The RcB method, which is based on BDM and CMT, is applied in M5. We observe that M4, which applies BDM without RcB, results in a -1.3 lower mAP than M5. Focusing on the defined rare classes, we see that RcB helps M5 to obtain +10.8 and +1.8 AP gains to the M4 in ‘Train’ and ‘Motorcycle’, respectively, and yields the best APs among all the models. By comparing the gains of mAP in ablative models, we conclude that among the three methods, the BDM is mostly beneficial for domain adaptation.

5 Conclusion

In this paper, we present a model named UDA4Inst that aims to address the challenge of synth-to-real UDA for instance segmentation in the field of autonomous driving. We introduce the three novel and effective methods in our model which are instance-level bidirectional data mixing, rare-class balancing, and category module training. In a comprehensive evaluation of three synth-to-real domain settings UrbanSyn \rightarrow Cityscapes, Synscapes \rightarrow Cityscapes, and SYNTHIA \rightarrow Cityscapes, we show that UDA4Inst achieves significant improvements in instance segmentation compared to the baseline model Mask2Former. This is the first work to provide competitive AP results on Synscapes and the recently published synthetic dataset UrbanSyn. Our proposed UDA4Inst model yields also state-of-the-art results on SYNTHIA. We look forward to the pro-

posed method will contribute to the development of UDA and can be widely served for future research.

Acknowledgments This work has been supported by the Spanish grant Ref. PID2020-115734RB-C21 (ADA/SSL-ADA subproject) funded by MCIN / AEI / 10.13039 / 501100011033. Yachan Guo acknowledges the financial support to her PhD from the Chinese Scholarship Council (CSC), grant number 202208310071. Antonio M. Lopez acknowledges the financial support to his general research activities given by ICREA under the ICREA Academia Program. All authors acknowledge the support of the Generalitat de Catalunya CERCA Program and its ACCIO agency to CVC’s general activities.

References

1. Aing, L., Lie, W.N., Lin, G.S.: Faster and finer pose estimation for multiple instance objects in a single rgb image. *Image and Vision Computing* **130**, 104618 (2023) [1](#)
2. Benbarka, N.: Instance Segmentation and 3D Multi-Object Tracking for Autonomous Driving. Ph.D. thesis, Universität Tübingen (2023) [1](#)
3. Biassetton, M., Michieli, U., Agresti, G., Zanuttigh, P.: Unsupervised domain adaptation for semantic segmentation of urban scenes. In: *CVPR Workshops (2019)* [2](#)
4. Bolya, D., Zhou, C., Xiao, F., Lee, Y.J.: Yolact: Real-time instance segmentation. In: *ICCV (2019)* [3](#)
5. Chen, J., Sun, M., Bao, T., Zhao, R., Wu, L., He, Z.: 3d model-based zero-shot pose estimation pipeline. *arXiv preprint arXiv:2305.17934* (2023) [1](#)
6. Cheng, B., Misra, I., Schwing, A.G., Kirillov, A., Girdhar, R.: Masked-attention mask transformer for universal image segmentation. In: *CVPR (2022)* [2](#), [3](#), [5](#), [9](#), [10](#)
7. Cheng, B., Schwing, A., Kirillov, A.: Per-pixel classification is not all you need for semantic segmentation. *NeurIPS* **34** (2021) [3](#)
8. Cordts, M., Omran, M., Ramos, S., Rehfeld, T., Enzweiler, M., Benenson, R., Franke, U., Roth, S., Schiele, B.: The cityscapes dataset for semantic urban scene understanding. In: *CVPR (2016)* [1](#), [8](#)
9. Deng, J., Li, W., Chen, Y., Duan, L.: Unbiased mean teacher for cross-domain object detection. In: *CVPR (2021)* [6](#)
10. Dosovitskiy, A., Beyer, L., Kolesnikov, A., Weissenborn, D., Zhai, X., Unterthiner, T., Dehghani, M., Minderer, M., Heigold, G., Gelly, S., et al.: An image is worth 16x16 words: Transformers for image recognition at scale. *arXiv preprint arXiv:2010.11929* (2020) [3](#)
11. Dosovitskiy, A., Ros, G., Codevilla, F., Lopez, A., Koltun, V.: Carla: An open urban driving simulator. In: *CoRL. PMLR (2017)* [2](#)
12. Ganin, Y., Ustinova, E., Ajakan, H., Germain, P., Larochelle, H., Laviolette, F., March, M., Lempitsky, V.: Domain-adversarial training of neural networks. *Journal of machine learning research* **17**(59), 1–35 (2016) [2](#)
13. Gao, L., Zhang, J., Zhang, L., Tao, D.: Dsp: Dual soft-paste for unsupervised domain adaptive semantic segmentation. In: *ACM Multimedia (2021)* [2](#), [4](#)
14. Garnett, N., Uziel, R., Efrat, N., Levi, D.: Synthetic-to-real domain adaptation for lane detection. In: *ACCV (2020)* [2](#)

15. Gómez, J.L., Silva, M., Seoane, A., Borrás, A., Noriega, M., Ros, G., Iglesias-Guitian, J.A., López, A.M.: All for one, and one for all: Urbansyn dataset, the third musketeer of synthetic driving scenes. arXiv preprint arXiv:2312.12176 (2023) [2](#), [8](#)
16. Gómez, J.L., Villalonga, G., López, A.M.: Co-training for deep object detection: Comparing single-modal and multi-modal approaches. *Sensors* **21**(9), 3185 (2021) [2](#)
17. Gómez, J.L., Villalonga, G., López, A.M.: Co-training for unsupervised domain adaptation of semantic segmentation models. *Sensors* **23**(2), 621 (2023) [2](#)
18. Gong, R., Li, W., Chen, Y., Gool, L.V.: Dlow: Domain flow for adaptation and generalization. In: CVPR (2019) [3](#)
19. Guo, H., Mao, Y., Zhang, R.: Mixup as locally linear out-of-manifold regularization. In: AAAI (2019) [4](#)
20. He, J., Jia, X., Chen, S., Liu, J.: Multi-source domain adaptation with collaborative learning for semantic segmentation. In: CVPR (2021) [2](#), [9](#)
21. He, K., Gkioxari, G., Dollár, P., Girshick, R.: Mask r-cnn. In: ICCV (2017) [3](#)
22. Hoffman, J., Tzeng, E., Park, T., Zhu, J.Y., Isola, P., Saenko, K., Efros, A., Darrell, T.: Cycada: Cycle-consistent adversarial domain adaptation. In: ICML. Pmlr (2018) [3](#)
23. Hoffman, J., Wang, D., Yu, F., Darrell, T.: Fcns in the wild: Pixel-level adversarial and constraint-based adaptation. arXiv preprint arXiv:1612.02649 (2016) [3](#)
24. Hoyer, L., Dai, D., Van Gool, L.: Daformer: Improving network architectures and training strategies for domain-adaptive semantic segmentation. In: CVPR (2022) [2](#), [3](#), [4](#), [6](#)
25. Hoyer, L., Dai, D., Van Gool, L.: Hrda: Context-aware high-resolution domain-adaptive semantic segmentation. In: ECCV. Springer (2022) [2](#), [3](#), [4](#), [6](#)
26. Hoyer, L., Dai, D., Wang, H., Van Gool, L.: Mic: Masked image consistency for context-enhanced domain adaptation. In: CVPR (2023) [2](#), [3](#), [6](#)
27. Huang, J., Guan, D., Xiao, A., Lu, S.: Cross-view regularization for domain adaptive panoptic segmentation. In: CVPR (2021) [2](#), [4](#), [10](#), [11](#)
28. Huang, J., Guan, D., Xiao, A., Lu, S., Shao, L.: Category contrast for unsupervised domain adaptation in visual tasks. In: CVPR (2022) [2](#), [4](#), [10](#)
29. Huang, K., Lertniphonphan, K., Chen, F., Li, J., Wang, Z.: Multi-object tracking by self-supervised learning appearance model. In: CVPR Workshops (2023) [1](#)
30. Huo, X., Xie, L., Zhou, W., Li, H., Tian, Q.: Focus on your target: A dual teacher-student framework for domain-adaptive semantic segmentation. arXiv preprint arXiv:2303.09083 (2023) [2](#), [4](#)
31. Jain, J., Li, J., Chiu, M.T., Hassani, A., Orlov, N., Shi, H.: Oneformer: One transformer to rule universal image segmentation. In: CVPR (2023) [3](#)
32. Kim, D., Seo, M., Park, K., Shin, I., Woo, S., Kweon, I.S., Choi, D.G.: Bidirectional domain mixup for domain adaptive semantic segmentation. In: AAAI (2023) [4](#)
33. Lewy, D., Mańdziuk, J.: An overview of mixing augmentation methods and augmentation strategies. *Artificial Intelligence Review* **56**(3), 2111–2169 (2023) [4](#)
34. Li, F., Zhang, H., Xu, H., Liu, S., Zhang, L., Ni, L.M., Shum, H.Y.: Mask dino: Towards a unified transformer-based framework for object detection and segmentation. In: CVPR (2023) [3](#)
35. Li, P., Ding, S., Chen, X., Hanselmann, N., Cordts, M., Gall, J.: Powerbev: A powerful yet lightweight framework for instance prediction in bird’s-eye view. arXiv preprint arXiv:2306.10761 (2023) [1](#)

36. Lin, T.Y., Maire, M., Belongie, S., Hays, J., Perona, P., Ramanan, D., Dollár, P., Zitnick, C.L.: Microsoft coco: Common objects in context. In: ECCV. Springer (2014) [9](#)
37. Liu, X., Han, Y., Bai, S., Ge, Y., Wang, T., Han, X., Li, S., You, J., Lu, J.: Importance-aware semantic segmentation in self-driving with discrete wasserstein training. In: AAAI (2020) [3](#)
38. Liu, Z., Lin, Y., Cao, Y., Hu, H., Wei, Y., Zhang, Z., Lin, S., Guo, B.: Swin transformer: Hierarchical vision transformer using shifted windows. In: ICCV (2021) [2](#), [9](#)
39. Long, M., Cao, Y., Wang, J., Jordan, M.: Learning transferable features with deep adaptation networks. In: ICML. PMLR (2015) [2](#)
40. Long, M., Cao, Z., Wang, J., Jordan, M.I.: Conditional adversarial domain adaptation. *NeurIPS* **31** (2018) [2](#)
41. Loshchilov, I., Hutter, F.: Decoupled weight decay regularization. arXiv preprint arXiv:1711.05101 (2017) [9](#)
42. Lu, Z., Yang, Y., Zhu, X., Liu, C., Song, Y.Z., Xiang, T.: Stochastic classifiers for unsupervised domain adaptation. In: CVPR (2020) [2](#)
43. Mattolin, G., Zanella, L., Ricci, E., Wang, Y.: Confmix: Unsupervised domain adaptation for object detection via confidence-based mixing. In: WACV (2023) [2](#)
44. de Melo, C.M., Torralba, A., Guibas, L., DiCarlo, J., Chellappa, R., Hodgins, J.: Next-generation deep learning based on simulators and synthetic data. *Trends in cognitive sciences* (2022) [2](#)
45. Nikolenko, S.I.: Synthetic data for deep learning, vol. 174. Springer (2021) [2](#)
46. Oza, P., Sindagi, V.A., Sharmini, V.V., Patel, V.M.: Unsupervised domain adaptation of object detectors: A survey. *IEEE TPAMI* (2023) [2](#)
47. Pan, Y., Yao, T., Li, Y., Wang, Y., Ngo, C.W., Mei, T.: Transferrable prototypical networks for unsupervised domain adaptation. In: CVPR (2019) [2](#)
48. Porzi, L., Hofinger, M., Ruiz, I., Serrat, J., Buló, S.R., Kotschieder, P.: Learning multi-object tracking and segmentation from automatic annotations. In: CVPR (2020) [1](#)
49. Ramachandran, P., Parmar, N., Vaswani, A., Bello, I., Levskaya, A., Shlens, J.: Stand-alone self-attention in vision models. *NeurIPS* **32** (2019) [3](#)
50. Ros, G., Sellart, L., Materzynska, J., Vazquez, D., Lopez, A.M.: The synthia dataset: A large collection of synthetic images for semantic segmentation of urban scenes. In: CVPR (2016) [8](#)
51. Rozantsev, A., Salzmann, M., Fua, P.: Beyond sharing weights for deep domain adaptation. *IEEE TPAMI* **41**(4), 801–814 (2018) [3](#)
52. Saha, S., Hoyer, L., Obukhov, A., Dai, D., Van Gool, L.: Edaps: Enhanced domain-adaptive panoptic segmentation. In: Proceedings of the IEEE/CVF International Conference on Computer Vision (ICCV). pp. 19234–19245 (October 2023) [2](#), [3](#), [4](#), [10](#), [11](#)
53. Saito, K., Watanabe, K., Ushiku, Y., Harada, T.: Maximum classifier discrepancy for unsupervised domain adaptation. In: CVPR (2018) [3](#)
54. Shan, Y., Lu, W.F., Chew, C.M.: Pixel and feature level based domain adaptation for object detection in autonomous driving. *Neurocomputing* **367**, 31–38 (2019) [2](#)
55. Sun, B., Feng, J., Saenko, K.: Return of frustratingly easy domain adaptation. In: AAAI (2016) [3](#)
56. Tranheden, W., Olsson, V., Pinto, J., Svensson, L.: Dacs: Domain adaptation via cross-domain mixed sampling. In: WACV (2021) [2](#), [3](#), [4](#), [6](#)

57. Tsai, Y.H., Hung, W.C., Schuler, S., Sohn, K., Yang, M.H., Chandraker, M.: Learning to adapt structured output space for semantic segmentation. In: CVPR (2018) [3](#)
58. Tseng, K.K., Lin, J., Chen, C.M., Hassan, M.M.: A fast instance segmentation with one-stage multi-task deep neural network for autonomous driving. *Computers & Electrical Engineering* **93**, 107194 (2021) [1](#)
59. Uddin, A., Monira, M., Shin, W., Chung, T., Bae, S.H., et al.: Saliencymix: A saliency guided data augmentation strategy for better regularization. arXiv preprint arXiv:2006.01791 (2020) [4](#)
60. Vaswani, A., Shazeer, N., Parmar, N., Uszkoreit, J., Jones, L., Gomez, A.N., Kaiser, Ł., Polosukhin, I.: Attention is all you need. *NeurIPS* **30** (2017) [3](#)
61. Vu, T.H., Jain, H., Bucher, M., Cord, M., Pérez, P.: Advent: Adversarial entropy minimization for domain adaptation in semantic segmentation. In: CVPR (2019) [3](#)
62. Walawalkar, D., Shen, Z., Liu, Z., Savvides, M.: Attentive cutmix: An enhanced data augmentation approach for deep learning based image classification. arXiv preprint arXiv:2003.13048 (2020) [4](#)
63. Wang, N., Shi, C., Guo, R., Lu, H., Zheng, Z., Chen, X.: Insmos: Instance-aware moving object segmentation in lidar data. arXiv preprint arXiv:2303.03909 (2023) [1](#)
64. Wang, Q., Dai, D., Hoyer, L., Van Gool, L., Fink, O.: Domain adaptive semantic segmentation with self-supervised depth estimation. In: ICCV (2021) [3](#)
65. Wong, K., Wang, S., Ren, M., Liang, M., Urtasun, R.: Identifying unknown instances for autonomous driving. In: CoRL. PMLR (2020) [1](#)
66. Wrenninge, M., Unger, J.: Synscapes: A photorealistic synthetic dataset for street scene parsing. arXiv preprint arXiv:1810.08705 (2018) [2](#), [8](#)
67. Yu, F., Wang, D., Chen, Y., Karianakis, N., Shen, T., Yu, P., Lymberopoulos, D., Lu, S., Shi, W., Chen, X.: Sc-uda: Style and content gaps aware unsupervised domain adaptation for object detection. In: WACV (2022) [2](#)
68. Yun, S., Han, D., Oh, S.J., Chun, S., Choe, J., Yoo, Y.: Cutmix: Regularization strategy to train strong classifiers with localizable features. In: ICCV (2019) [4](#)
69. Zhang, H., Cisse, M., Dauphin, Y.N., Lopez-Paz, D.: mixup: Beyond empirical risk minimization. arXiv preprint arXiv:1710.09412 (2017) [4](#)
70. Zhang, H., Tian, Y., Wang, K., He, H., Wang, F.Y.: Synthetic-to-real domain adaptation for object instance segmentation. In: International Joint Conference on Neural Networks (IJCNN). IEEE (2019) [2](#), [4](#), [10](#), [11](#)
71. Zhao, H., Jia, J., Koltun, V.: Exploring self-attention for image recognition. In: CVPR (2020) [3](#)